Article ID:1004-4213(2010)10-1857-4

Light Propagation in a Circular Double Clad Fiber Using Coupled Mode Method

XU Zhong-nan, LIU Ze-jin

(*College of Optoelectronic Science and Engineering, National University of Defense Technology, Changsha* 410073, *China*)

Abstract:For better understanding the light propagation in a double clad fiber (DCF), the perfect circular double clad fiber is numerically investigated by using the coupled mode method with translating the DCF into a single mode fiber (SMF) and an annular core fiber (ACF). The coupling coefficients between the LP_{01} mode of the SMF and the guided modes of the ACF are calculated. The results show that the LP_{0n} modes of the ACF have greater coupling coefficients than the other guided modes, and for the LP_{0n} modes the coupling coefficient of the high-order mode is larger than that of the low-order mode. The field distribution in the DCF core calculated by the coupled mode equations shows a quasi-periodic distribution along the DCF. The average period of the field distribution increases with the increasing of wavelength for different DCF parameters and the average normalized power of the field distribution is closely related to the chosen parameters of the DCF.

Key words:Double clad fiber(DCF); Single clad fiber(SCF); Annular core fiber(ACF); Coupled mode theory

CLCN:O43; TN **Document Code**:A **doi**:10.3788/gzxb20103910.1857

0 Introduction

Fiber technology has attracted significant interests during the last decades. The appearance of DCFs provides an efficient way to generate high power fiber laser[1-3]. In comparison with other types of fiber, DCFs benefit from their large inner cladding which result in a large effective mode area and a high numerical aperture. Light propagation in DCFs has been theoretically studied by using the methods of ray tracing[4], wave-optical approach[5] and eigenmode expansion[6]. According to the eigenmode expansion method, the light propagation in a perfect circular DCF is explained by the propagation of a complete set of guided modes, so the field distribution is uniform along the DCF.

In this paper, we use the coupled mode theory[7-8] to study the light propagation in the perfect circular DCF with translating it into two coupled fibers: a SMF and an ACF[9-11]. We obtain the LP_{01} mode of the SMF and the guided modes of the ACF at different wavelengths, and then calculate the coupling coefficients of the modes between the two fibers. The results show that the modes with the same symmetry can be strongly coupled between the two fibers. For the ACF the LP_{0n} modes have greater coupling coefficients than the other guided modes, and for the LP_{0n} modes the coupling coefficients of the high-order mode are larger than those of the low-order mode. With considering all the LP_{0n} guided modes of the ACF, the field distribution in the DCF core is calculated at different wavelengths by using the coupled mode equations. From the calculated results we find that the power in the core shows a quasi-periodic distribution along the DCF, the average period of the distribution increases with increasing of wavelength for different DCF parameters, and the average power in the core is closely related to the chosen parameters.

1 Theoretical formulation

Coupled mode theory has been widely used to analyze the light propagation in fiber couplers[7] and that in multicore fibers[12]. In this paper, we use coupled mode theory to study the light propagation in the perfect circular DCF by translating it into a single clad fiber (SCF) and an ACF. The refractive index profiles for the DCF, the SCF and the ACF are schematically shown in Fig. 1. The refractive indices have $n_1 > n_2 > n_3$ and the outer cladding radii of the three fibers are infinite.

Tel:029-88887617 Email:xznwork@163.com
Received date:2010-04-20 Revised date:2010-07-12

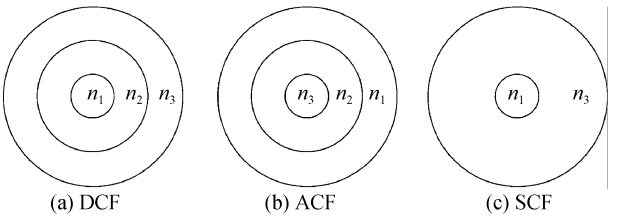

Fig. 1 Schemes for the DCF, the ACF and the SCF

1.1 Eigenmodes of the SCF and the ACF

Due to the slight refractive index differences of $\Delta n_{12}=n_1-n_2$ and $\Delta n_{13}=n_1-n_3$, the eigenmodes of the SCF and the ACF are transformed into linear polarization modes by using weakly guiding approximation[13], which are expressed as LP_{mn} ($m \geqq 0$, $n>0$) modes. The distribution of the LP_{mn} mode of the SCF is expressed as

$$E^{S}_{x,y}=\begin{cases} B_1 J_m(h_S r)\mathrm{e}^{\mathrm{i}m\varphi}\exp[\mathrm{i}(\omega t-\beta z)] & r\leqslant a \\ B_2 K_m(q_S r)\mathrm{e}^{\mathrm{i}m\varphi}\exp[\mathrm{i}(\omega t-\beta z)] & a<r \end{cases} \tag{1}$$

where J_m and K_m denote the Bessel functions of the first and second (modified) kinds of order m, respectively. $h_S=[(k_0 n_1)^2-\beta^2]^{1/2}$, $q_S=[\beta^2-(k_0 n_3)^2]^{1/2}$, a is the core radius of the DCF, n_1 and n_3 are the refractive indices as shown in Fig. 1(b), and β is the propagation constant and satisfies the eigenvalue equation

$$h_S\frac{J_{m+1}(h_S a)}{J_m(h_S a)}=q_S\frac{K_{m+1}(h_S a)}{K_m(h_S a)} \tag{2}$$

The relation between B_1 and B_2 is determined by the boundary condition.

For the ACF the transversal distribution of the LP_{mn} mode can be expressed as[9]

$$E^{A}_{x,y}=\begin{cases} A_1 I_m(q_A r)\mathrm{e}^{\mathrm{i}m\varphi}\exp[\mathrm{i}(\omega t-\beta z)] & (r\leqslant a) \\ [A_2 J_m(h_A r)+A_3 Y_m(h_A r)]\mathrm{e}^{\mathrm{i}m\varphi}\cdot \\ \quad \exp[\mathrm{i}(\omega t-\beta z)] & (a<r<b) \\ A_4 K_m(q_A r)\mathrm{e}^{\mathrm{i}m\varphi}\exp[\mathrm{i}(\omega t-\beta z)] & (b\leqslant r) \end{cases} \tag{3}$$

where I_m and Y_m denote the Bessel functions of the first (modified) and second kinds of order m, respectively. $h_A=[(k_0 n_2)^2-\beta^2]^{1/2}$, $q_A=[\beta^2-(k_0 n_3)^2]^{1/2}$, n_2 and n_3 are the refractive indices as shown in Fig. 1(c), and b is the inner cladding radius of the DCF. By using boundary conditions we can obtain

$$S\cdot(A_1 A_2 A_3 A_4)^T=0 \tag{4}$$

where

$$S=\begin{vmatrix} I_m(q_A a) & -J_m(h_A a) & -Y_m(h_A a) & 0 \\ q_A I_{m+1}(q_A a) & h_A J_{m+1}(h_A a) & h_A Y_{m+1}(h_A a) & 0 \\ 0 & J_m(h_A b) & Y_m(h_A b) & -K_m(q_A b) \\ 0 & h_A J_{m+1}(h_A b) & h_A Y_{m+1}(h_A b) & -q_A K_{m+1}(q_A b) \end{vmatrix} \tag{5}$$

Then the eigenvalue equation for the ACF can be obtained by setting the determinant of the matrix S to zero.

The ACF can support several eigenmodes at a given wavelength. To judge the mode number, a parameter named normalized frequency V is introduced, which is defined as follow[13]

$$V=k_0 a\sqrt{n_2^2-n_3^2}=2\pi a/\lambda\cdot\sqrt{n_2^2-n_3^2} \tag{6}$$

where λ is the wavelength, then we can obtain the eigenvalue equation for V with setting $q_A=0$ as follows

$$J_{m-1}(V)Y_{m-1}(V\cdot b/a)-J_{m-1}(V\cdot b/a)Y_{m-1}(V)=0 \tag{7}$$

1.2 Coupled mode equations

For a system of parallel lossless fibers, each equation of the set of coupled mode equations can be expressed as[7]

$$\frac{\mathrm{d}\alpha_p^{(j)}}{\mathrm{d}z}+\mathrm{i}\beta_p^{(j)}\alpha_p^{(j)}=\mathrm{i}\sum_{\substack{s=1\\ s\neq j}}^{n}\sum_q C_{pq}^{(j)(s)}\alpha_q^{(s)} \tag{8}$$

where $\beta_p^{(j)}$ is the propagation constant of the pth mode in fiber j and $C_{pq}^{(j)(s)}$, the coupling coefficient between the pth mode in fiber j and the qth mode in fiber s, is given by

$$C_{pq}^{(j)(s)}=\frac{\omega}{2}\int_{-\infty}^{+\infty}\int(\varepsilon-\varepsilon^{(s)})\mathrm{e}_p^{(j)}\cdot\mathrm{e}_q^{(s)}\,\mathrm{d}x\mathrm{d}y \tag{9}$$

where $\varepsilon^{(s)}$ is the fiber dielectric constant of fiber s, $\mathrm{e}_p^{(j)}$ and $\mathrm{e}_q^{(s)}$ are the orthogonal modes of the fiber j and fiber s, respectively. For one of the fibers, such as fiber j, the transverse field can be written as

$$E_t^{(j)}(x,y,z)=\sum_p \alpha_p^{(j)*}(z)\mathrm{e}_p^{(j)}(x,y) \tag{10}$$

where $\alpha_p^{(j)}$ is the amplitude of the pth mode in fiber j as in Eq. (8).

2 Numerical results and discussion

The refractive index profile of the DCF is schematically shown in Fig. 1(a) with a core radius of $a=4$ μm and an inner cladding radius of $b=60$ μm. The refractive index of the DCF's core is $n_1=1.444$. For simplicity the refractive index differences for the inner cladding and the outer cladding are chosen to be $\Delta n_{12}=0.000\,4$ and $\Delta n_{13}=0.001$, respectively, which ensures the SCF be a SMF due to the normalized frequency $V<2.405$[13] in the range of $\lambda=0.6$ to 1.1 μm.

We calculate the LP_{01} mode of the SMF by

using Eqs. (1) and (2) and the LP_{mn} (m, n=1, 2, 3) modes of the ACF by using Eqs. (3)～(5) in the range of λ=0.6 to 1.1 μm, respectively, and then the coupling coefficients between the two fibers are obtained by using Eq. (9) as shown in Fig. 2(The solid, dash and dot lines correspond to n=1, n=2, and n=3, respectively).

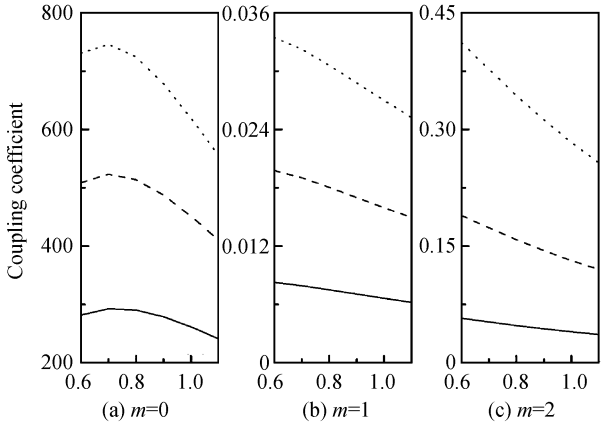

Fig. 2　Coupling coefficients between the LP_{01} mode of the SMF and the LP_{mn} modes of the ACF for m=0, m=1, and m=2, respectively

From Fig. 2, it can be seen that the coupling coefficients of the LP_{0n} modes are significantly larger than that of the LP_{1n} modes and the LP_{2n} modes for the ACF, so the LP_{01} mode of the SMF is mainly coupled with which of the ACF has the same symmetry. And for the LP_{0n} modes of the ACF, the coupling coefficient of the high-order mode is larger than that of the low-order mode, which can be explained by the mode distributions in the fiber profile. Due to the uniform angular distribution of the LP_{0n} modes, we plot only the power density along the X axis in the range of −60 μm to 60 μm for λ = 1.1 μm as shown in Fig. 3. Specially, the power density is divided by the power (in the ACF profile) of the related mode, which is necessary in the calculation of coupling coefficients . From Fig. 3 it can be seen

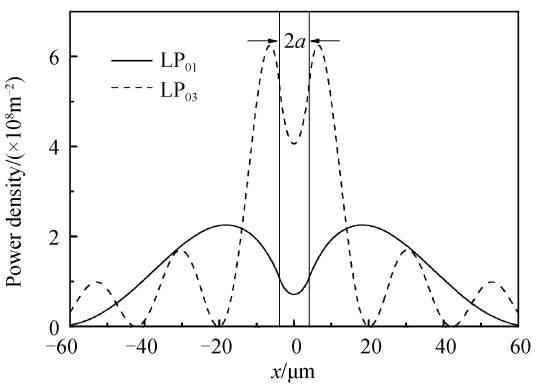

Fig. 3　Power density of the LP_{01} mode and the LP_{03} mode for the ACF

that the LP_{03} mode has larger power density than the LP_{01} mode in the core area for the ACF. Because the power of the LP_{01} mode of the SMF mainly locates in the DCF′s core, the LP_{03} mode of the ACF strongly couples with it. It can also be seen that the power density of the LP_{03} mode is more closed to the core area than that of the LP_{01} mode for the ACF. In what follows, we consider only the LP_{0n} modes for the ACF in the simulation.

From the above results we know that the complete set of guided modes for the ACF should be taken into account in the coupling of the modes between the SMF and the ACF. To judge the number of the guided modes of the ACF, Eq. (7) should be used. For examples, we denote the left-hand side of Eq. (7) as T and calculate its absolute value $|T|$ versus the normalized frequency V for λ=0.6 μm and 1.1 μm, respectively, as shown in Fig. 4. The maximum value of V is given by Eq. (6). Each zero point in Fig. 4 represents one guided mode of the ACF.

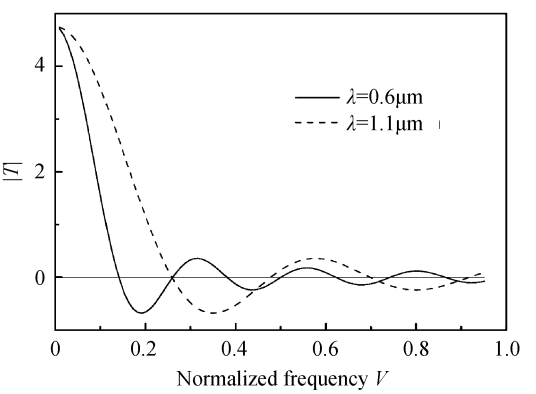

Fig. 4　Relation between $|T|$ and the normalized frequency V

We set the LP_{01} mode of the SMF to the initial field with power of P_{in} and then calculate the field distribution in the DCF core (P_{core}) along the Z axis from 0 to 8 cm in the range of λ = 0.6 to 1.1 μm by using Eqs. (8)～(10). Fig. 5(a) and (b) show the power along the Z axis for λ = 0.6 μm and 1.1 μm, respectively. It can be seen that the power shows a quasi-periodic distribution along the Z axis and the average period for λ = 0.6 μm is significantly smaller than that for λ = 1.1 μm. The average values of P_{core}/P_{in} are 0.184 and 0.339 for λ = 0.6 μm and 1.1 μm, respectively. It can also be found that the power continually translation between the core and the inner cladding.

For simplicity we maintain the DCF core radius a and the refractive index difference Δn_{13}, i.e., the SCF is still a SMF, and calculate the

average period and the average power in the DCF core with varying its parameters: the inner cladding radius b and the refractive index difference Δn_{12}. Fig. 6 shows the average periods of the power versus wavelength in the range of $\lambda=0.6$ to 1.1 μm with $b=20$ μm, 60 μm and 100 μm, respectively. In Fig. 6 the average periods increase with increasing of wavelength for $b=20$ μm, 60 μm and 100 μm, the average period increases for $b=20$ μm is slower than that for $b=60$ μm and that for $b=100$ μm, and the average periods are similar

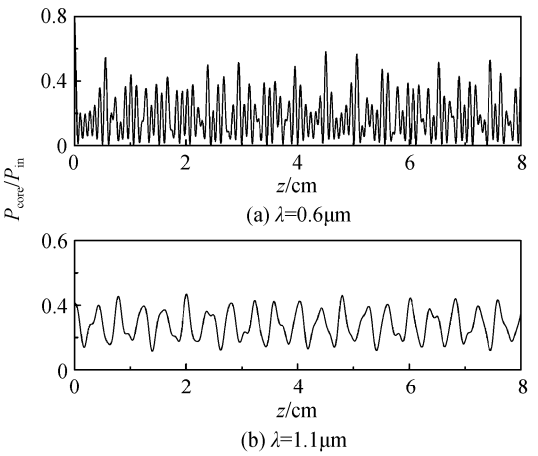

Fig. 5 Power distribution in the DCF core along the Z axis from 0 to 8 cm for $\lambda=0.6$ μm and $\lambda=1.1$ μm, respectively

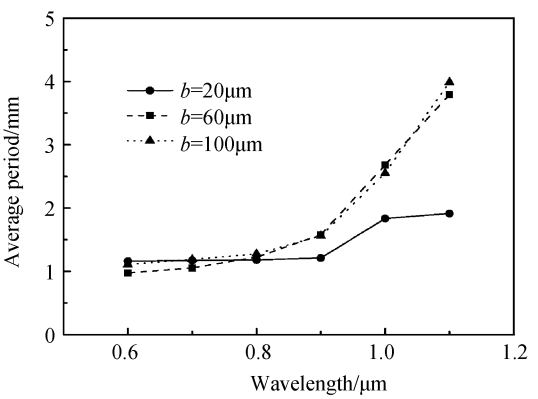

Fig. 6 Average period of the power in the DCF core for $b=20$ μm, 60 μm and 100 μm, respectively

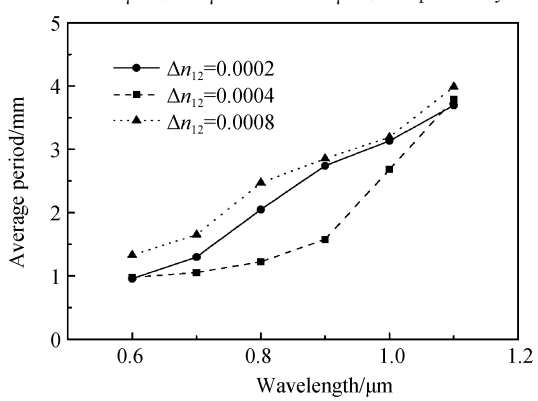

Fig. 7 Average period of the power in the DCF core for $\Delta n_{12}=0.000\,2$, $0.000\,4$ and $0.000\,8$, respectively

for $b=60$ μm and 100 μm. Fig. 7 shows the average periods of the power versus wavelength in the range of $\lambda=0.6$ to 1.1 μm with $\Delta n_{12}=0.000\,2$, $0.000\,4$ and $0.000\,8$, respectively, from which it can be seen that the average periods increase with increasing of wavelength for $\Delta n_{12}=0.000\,2$, $0.000\,4$ and $0.000\,8$. But from the results it also can be found that the average powers are closely related to the inner cladding radius for the DCF.

3 Conclusion

We have numerically investigated the light propagation in the perfect circular DCF by using the coupled mode method with translating it into two coupled fibers: a SMF and an ACF. According to the obtained guided modes of the SMF and the ACF, the coupling coefficients between them are calculated and the results show that the LP_{0n} modes of the ACF have greater coupling coefficients than the other guided modes, and for the LP_{0n} modes the coupling coefficient of the high-order mode is larger than that of the low-order mode. By using the coupled mode equations, the field distribution in the DCF core is calculated. From the results we find that the field shows a quasi-periodic distribution along the DCF, the average period of the distribution increases with increasing of wavelength for different inner cladding radii and different refractive indices of the inner cladding, and the average power is closely related to the parameters of the DCF. The results in this paper are useful for analyzing DCF and DCF devices.

References

[1] WANG Yi-shan, ZHENG Yao-lei, SHEN Hua, *et al*. High-efficiency generation of cladding pumped erbium-ytterbium co-doped double clad fiber laser[J]. *Acta Photonica Sinica*, 2003, **32**(9): 1025-1027.

[2] LI Jian-feng, DUAN Kai-liang, WANG Yi-shan, *et al*. Theoretical analysis of the heat dissipation mechanism in Yb^{3+}-doped double-clad fiber lasers[J]. *J mod Optics*, 2008, **55**(3): 459-471.

[3] DUAN Kai-liang, ZHAO Bao-yin, ZHAO Wei, *et al*. 1 000 W all fiber laser[J]. *Chinese Journal of Lasers*, 2009, **36**(12): 3219.

[4] LIU An-ping, UEDA K. The absorption characteristics of circular, offset, and rectangular double-clad fibers[J]. *Opt Commun.*, 1996, **132**(5-6): 511-518.

[5] HAUTAKORPI M, KAIVOLA M. Modal analysis of the self-imaging phenomenon in optical fibers with an annular core [J]. *Appl Opt*, 2006, **45**(25): 6388-6392.

[6] MONERIE M. Propagation in doubly clad single-mode fibers [J]. *IEEE Trans on Microw Theory Tech*, 1982, **MIT-30**(4): 381-388.

[7] MCINTYRE P D, SNYDER A W. Power transfer between

optical fibers[J]. *JOSA*, 1973, **63**(12): 1518-1527.
[8] HUANG Wei-ping, MU Jian-wei. Complex coupled-mode theory for optical waveguides[J]. *Opt Express*, 2009, **17**(21): 19134-19152.
[9] SARKAR B C, CHOUDHURY P K, YOSHINO T. On the analysis of a weakly guiding doubly clad dielectric optical fiber with an annular core[J]. *Microwave Opt Technol Lett*, 2001, **31**(6): 435-439.
[10] MARCOU J, FE′VRIER S. Comments on "on the analysis of a weakly guiding doubly clad dielectric optical fiber with an annular core"[J]. *Microwave and Optical Tech Lett*, 2003, **38**(3): 249-254.
[11] HAUTAKORPI M, KAIVOLA M. Modal analysis of M-type- dielectric-profile optical fibers in the weakly guiding approximation[J]. *JOSA A*, 2005, **22**(6): 1163-1169.
[12] BOCHOVE E J, CHEO P K, KING G G. Self-organization in a multicore fiber laser array[J]. *Opt Lett*, 2003, **28**(14): 1200-1202.
[13] AGRAWAL G P. Nonlinear fiber optics[M]. 3rd ed. New York: Academic Press, 2001: 36-37.

应用耦合模理论研究光在圆对称双包层光纤中的传输

徐中南，刘泽金
（国防科学技术大学 光电科学与工程学院，长沙 410073）

摘　要：为了深入理解双包层光纤的光场传输特性，应用耦合模理论将双包层光纤等效为相互耦合的单模光纤和环形芯光纤，研究了圆对称的双包层光纤的光场传输. 通过计算单模光纤 LP_{01} 模和环形芯光纤导模的耦合系数发现了环形芯光纤 LP_{0n} 模的耦合系数远大于其它导模的耦合系数，且 LP_{0n} 模中的高阶模比低阶模的耦合系数大. 据此，应用耦合模理论计算得到了该双包层光纤的光传输特性，计算结果发现光场沿光纤轴向呈近似周期分布，且纤芯中光功率变化的平均周期随波长递增，但平均归一化功率与光纤参数紧的选择有关.

关键词：双包层光纤；单包层光纤；环形芯光纤；耦合模理论

XU Zhong-nan　was born in 1980. He is currently working toward the Ph. D. degree at College of Optoelectronic Science and Engineering, National University of Defense Technology and his research interests focus on optical fibers and fiber devices.

LIU Ze-jin　was born in 1963. Now he is a professor of the College of Optoelectronic Science and Engineering, National University of Defense Technology, and his research interests focus on high power laser technology.